

# Standing Swells Surveyed Showing Surprisingly Stable Solutions for the Lorenz '96 Model

Morgan R. Frank<sup>1</sup>, Lewis Mitchell<sup>2</sup>, Christopher M. Danforth<sup>3</sup>

Computational Story Lab, Department of Mathematics and Statistics, Vermont Complex Systems Center, Vermont Advanced Computing Core,

University of Vermont, Burlington, Vermont

<sup>1</sup>mrfank@uvm.edu, <sup>2</sup>lmitchell@uvm.edu, <sup>3</sup>cdanfort@uvm.edu

July 19, 2022

**The Lorenz '96 model is an adjustable dimension system of ODEs exhibiting chaotic behavior representative of dynamics observed in the Earth's atmosphere. In the present study, we characterize statistical properties of the chaotic dynamics while varying the degrees of freedom and the forcing. Tuning the dimensionality of the system, we find regions of parameter space with surprising stability in the form of standing waves traveling amongst the slow oscillators. The boundaries of these stable regions fluctuate regularly with the number of slow oscillators. These results demonstrate hidden order in the Lorenz '96 system, strengthening the evidence for its role as a hallmark representative of nonlinear dynamical behavior.**

## 1 Introduction

Modern society often depends on accurate weather forecasting for daily planning, efficient air-travel, and disaster preparation [1]. Predicting the future state of physical systems, such as the atmosphere, proves to be difficult; chaotic systems exhibit sensitive dependence on initial conditions, meaning that small errors in any state approximation will lead to exponential error growth [2]. Furthermore, weather prediction requires the use of computationally expensive numerical models for representing the atmosphere. Most scientists trying to advance current predictive techniques can not afford to run these real-world weather models. To this end, computationally manageable “simple models” are used instead to represent interesting atmospheric characteristics while reducing the overall computation costs.

Scientists have long wrestled with chaotic behavior limiting the predictability of weather in the Earth's atmosphere [3–7]. In the case of atmospheric predictions, toy models exhibiting exponential error growth provide

an ideal environment for basic research in predictability. Edward Lorenz, one of the great pioneers in predictability research, introduced the following  $I$ -dimensional model which exhibits chaotic behavior when subject to sufficient forcing

$$\frac{dx_i}{dt} = x_{i-1}(x_{i+1} - x_{i-2}) - x_i + F \quad (1)$$

where  $i = 1, 2, \dots, I$  and  $F$  is the forcing parameter. Each  $x_i$  can be thought of as some atmospheric quantity, e.g. temperature, evenly distributed about a given latitude of the globe, hence there is a modularity in the indexing that is described by  $x_{i+I} = x_{i-I} = x_i$ .

In an effort to produce a more realistic growth rate of the large-scale errors, Lorenz went on to introduce a multi scale model by coupling two systems similar to the model in equation (1), but differing in time scales. The equations for the Lorenz '96 model [8] are given as

$$\frac{dx_i}{dt} = x_{i-1}(x_{i+1} - x_{i-2}) - x_i + F - \frac{hc}{b} \sum_{j=1}^J y_{(j,i)} \quad (2)$$

$$\frac{dy_{(j,i)}}{dt} = cby_{(j+1,i)}(y_{(j-1,i)} - y_{(j+2,i)}) - cy_{(j,i)} + \frac{hc}{b} x_i \quad (3)$$

where  $i = 1, 2, \dots, I$  and  $j = 1, 2, \dots, J$ . The parameters  $b$  and  $c$  indicate the time scale of solutions to equation (3) relative to solutions of equation (2), and  $h$  is the coupling parameter. The coupling term can be thought of as a parameterization of dynamics occurring at a spatial and temporal scale unresolved by the  $x$  variables. Again, each  $x_i$  can be thought of as an atmospheric quantity about a latitude that oscillates in slow time, and the set of  $y_{(j,i)}$  are a set of  $J$  fast time oscillators that act as a damping force on  $x_i$ . The  $y$ 's exhibit a similar modularity described by  $y_{(j+IJ,i)} = y_{(j-IJ,i)} = y_{(j,i)}$ . A snapshot of a solution state is shown as an example in Figure 1.

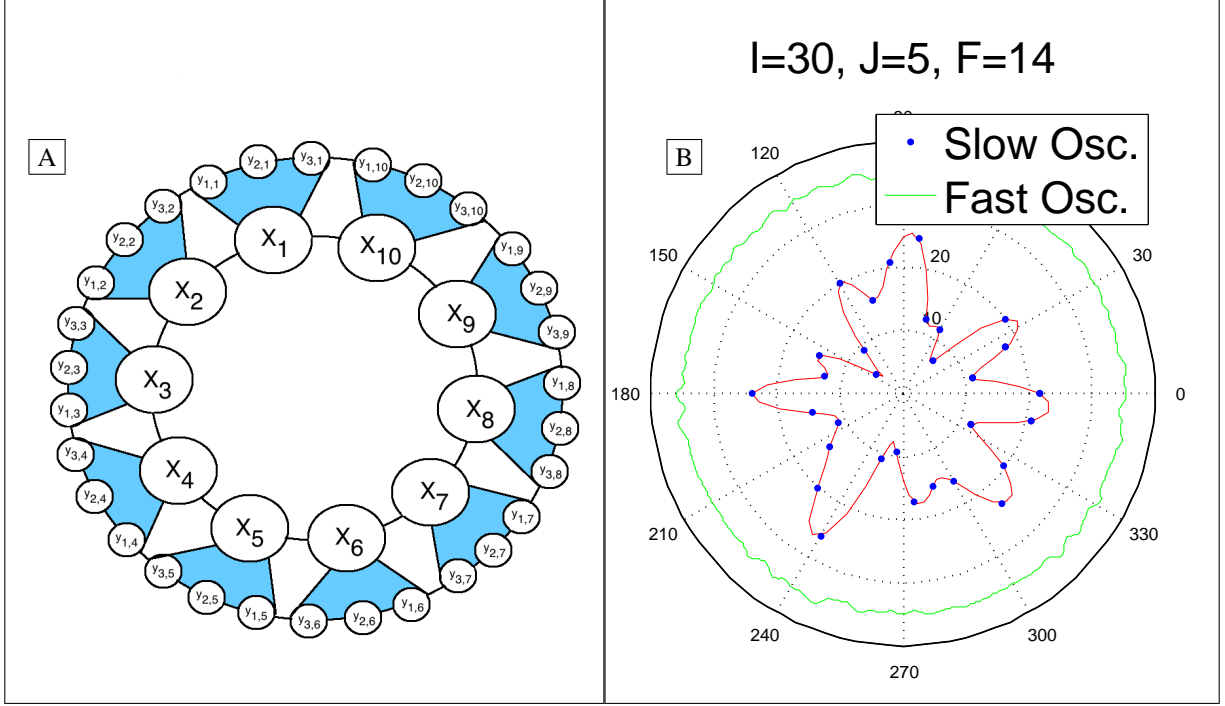


Figure 1. (A) A visual representation for the coupling of the fast and slow time systems in the Lorenz '96 model. There are  $I = 10$  slow large amplitude oscillators, each of which are coupled to  $J = 3$  fast small amplitude oscillators. The slow oscillators are arranged in a circle representing a given latitude. (B) An example snapshot from an actual trajectory with  $I = 30$ ,  $J = 5$ , and  $F = 14$ . The blue dots represent the slow oscillators, and the green represents the flow of information among the fast oscillators. See Figure 5 for further examples and a more detailed explanation.

This system has been used to represent weather related dynamics in several previous studies as a low-dimensional model of atmospheric dynamics [9–12]. There are many advantages to using the Lorenz '96 model. A primary advantage is that the model allows for flexibility in parameter tuning to achieve varying relative levels of nonlinearity, coupling of timescales, and spatial degrees of freedom. Unless otherwise noted, we fix the time scaling parameters  $b = c = 10$  and the coupling parameter  $h = 1$  for the remainder of this study. These parameter choices are consistent with the literature in terms of producing chaotic dynamics quantitatively similar to those observed in the atmosphere [13]. We vary  $I$ ,  $J$ , and  $F$  to explore different spatial degrees of freedom and different levels of nonlinearity in the system dynamics.

In this study, we characterize the parameter space of the Lorenz '96 system revealing patterns of order and chaos in the system. We discuss our methods in Section 2. In Section 3 and 4, we provide our results along with evidence for stability in the Lorenz '96 model in the form of standing waves traveling around the slow oscillators. We discuss the implications of our findings in Section 4.

## 2 Methods

We examine the Lorenz '96 model for forcings  $F \in [1, 18]$ , and integer spatial dimensions  $I \in [4, 50]$  and  $J \in [0, 50]$ . For each choice of  $F$ ,  $I$ , and  $J$ , we integrate the Lorenz '96 model with a randomly selected initial condition in the basin of attraction for the system attractor. We use the Runge-Kutta method of order-4 [14] with a time step of .001 to integrate the initial point along its trajectory. Initially, we iterate the point 500 time units without performing any analysis so that the trajectory is allowed to approach the attractor; thus transient activity will be ignored. From here, we integrate an additional 500 time units for analysis. Results were insensitive to increases in integration time, specific choices of initial condition, and decreases in time step. Examples of stable and chaotic trajectories are shown in Figure 2.

We use the largest Lyapunov exponent, the percentage of positive Lyapunov exponents, and the normalized Lyapunov dimension to characterize the nonlinearity of the system. We approximate the Lyapunov exponent for the

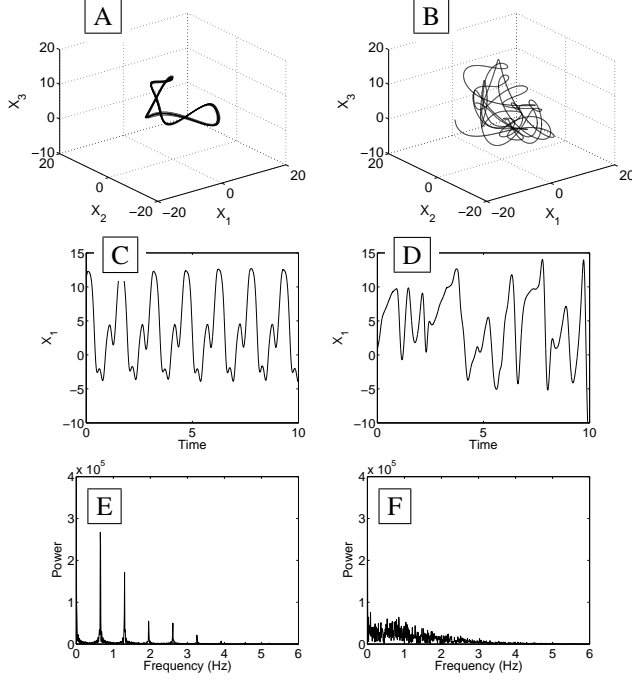


**Figure 2.** Two example trajectories of the Lorenz '96 model, along with periodograms for the corresponding trajectories of the slow oscillators. (A, C, & E)  $I = 4$ ,  $J = 8$ , and  $F = 14$ . We observe a fairly regular trajectory. The periodogram for this system supports this by showing that only a few isolated frequencies have significant power. (B, D, & F)  $I = 10$ ,  $J = 5$ , and  $F = 14$ . We observe an irregular trajectory. The periodogram exhibits some power at many frequencies.

$i$ th dimension of the slow modes  $X$  along the trajectory  $\vec{v}$  as

$$L_i(v) \approx \frac{1}{\Delta \text{time}_{\text{total}}} \sum_{n=1}^N \ln(|f(\vec{v}_i^{(n)})|) \quad (4)$$

where  $N$  is the number of iterations,  $\vec{v}_i^{(n)}$  is the  $i$ th coordinate of the trajectory at the  $n$ th iterate,  $\Delta \text{time}_{\text{total}}$  is the total model time, and  $f$  is the stretch factor measured from the trajectories of an  $I$ -dimensional ensemble near a point on the trajectory over a unit time step. This calculation can be thought of as an average of the natural-log of the stretching/shrinking dynamics of the system acting on an ensemble of points very near to the trajectory over time. The Lyapunov dimension is given by

$$L = D + \frac{1}{|L_{D+1}(\vec{v})|} \sum_{d=1}^D L_d(\vec{v}) \quad (5)$$

where  $D$  is the largest whole number such that  $\sum_{d=1}^D L_d(\vec{v}) \geq 0$ . This calculation yields an approximation of the slow mode attractor fractal dimension. In general,

the fractal dimension compared to the number of slow mode dimensions in the model (namely  $I$ ) provides a reasonable measure of the nonlinearity in the system which we can subsequently compare to the dynamics resulting from different parameter choices [15].

From the one-dimensional time series in Figure 2, we see examples of the dynamics exhibited by the slow variables  $X$  ( $x_1$  is a representative example of  $X$ ). We also measure nonlinearity by looking at the frequency spectrum for the trajectories of individual slow oscillators. Given a time series, the frequency spectrum can be approximated using the Fourier transform [16, 17]. Chaotic systems typically exhibit power at a large number of frequencies, while stable systems will exhibit power at only a small number of frequencies. Furthermore, the frequency spectrum illuminates which frequencies the  $X$  variables will tend to exhibit.

Lorenz suggested that the slow oscillators represent measurements of some atmospheric quantity about a given latitude [8]. With this in mind, it is meaningful to visualize the system accordingly. Different from the images provided in Figure 2, we will visualize states for all of the slow oscillators during a given trajectory as points evenly spaced around a circle centered at the origin, where the origin represents the lowest value ( $x_{\min}$ ) obtained by any of the slow oscillators along their respective trajectories. Each point's distance from the origin is given by  $x_i$ 's current value minus  $x_{\min}$ . Treating the points in polar-coordinates  $(r, \theta)$ , where  $r$  is the oscillator's distance from  $x_{\min}$  and  $\theta$  indicates the subscript of the oscillator, we fit a cubic spline to the shifted slow oscillator values to obtain approximations for the flow of the atmospheric quantity between the slow oscillators. For clarity, the slow oscillators' radial positions ( $\theta$ ) remain fixed, while their distance from the origin varies over the course of the trajectory (see Fig. 1B). Note that this method of visualization allows us to observe all of the slow oscillators at once for any state on a trajectory. A similar method is performed to represent the activity of the fast oscillators in the same plot (the outer ring).

### 3 Results

It is common in the literature referencing the Lorenz '96 model to see the parameters  $I$ ,  $J$ , and  $F$  chosen to ensure that the system exhibits sufficient amounts of chaos to make the prediction problem interesting. For example, it is well-known that  $F > 6$  will usually result in a weakly chaotic system for reasonable choices of  $I$  and  $J$  [9, 13].

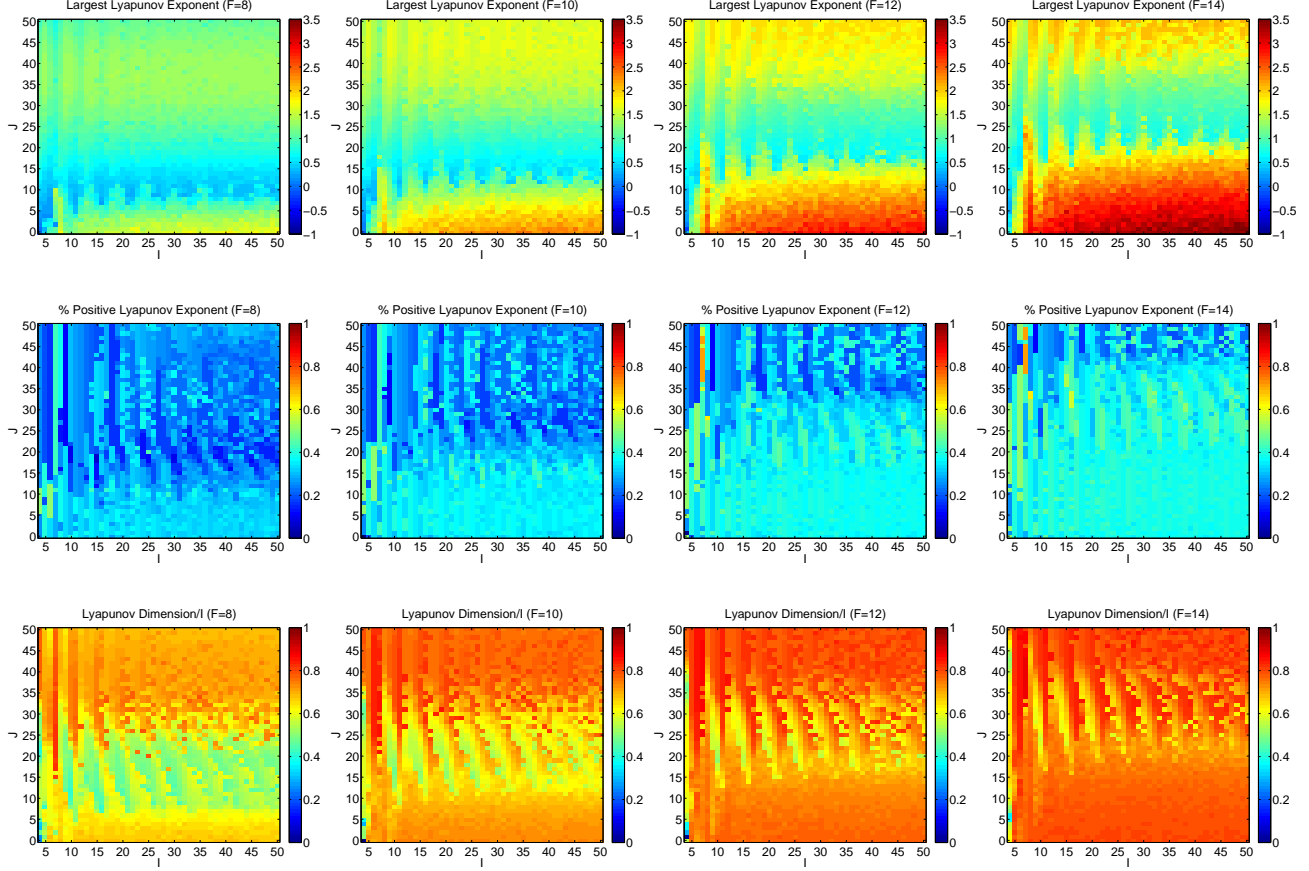


**Figure 3.** For these plots, the axes represent integer values of the model dimensions  $I$  (slow) and  $J$  (fast). Each cell in the resulting plot represents a single integration with 500 unit time steps (or  $10^6$  iterations) of the Lorenz '96 model. Note that these images are insensitive to changes in initial condition. (Far Left Column)  $F = 8$ . (Center Left Column)  $F = 10$ . (Center Right Column)  $F = 12$ . (Far Right Column)  $F = 14$ . (Top Row) The largest Lyapunov exponent. (Middle Row) The percent of positive Lyapunov exponents. (Bottom Row) The normalized Lyapunov dimension.

Beyond this,  $I = 8$  and  $J = 4$  for a total of 40 oscillators is a popular choice, so much so that it is commonly known as the “Lorenz 40-variable” model [18]. Generalizing from these standards, we explore the parameter space for  $I$ ,  $J$ , and  $F$  systematically and characterize the resulting dynamical systems.

We first measure the largest Lyapunov exponent for several choices of  $I$ ,  $J$ , and  $F$  in Figure 3 (top row). We observe that the lower portion of the plots (i.e. small  $J$ ) exhibit strong, positive largest Lyapunov exponents (red & yellow regions). As  $J$  is increased, we observe the emergence of greatly reduced largest Lyapunov exponent (blue regions). This region of reduced chaotic activity returns to a region of increased largest Lyapunov exponent as we continue to increment  $J$ . Furthermore, we observe that the top and bottom borders of the blue regions oscillate with increasing  $I$ . The blue region of reduced chaos appears

to occur at larger values of  $J$  as  $F$  is increased, while the range of the blue regions remain fairly constant in  $J$ .

We observe the percentage of positive Lyapunov exponents in the middle row of Figure 3. Green vertical windows of increased percentage of positive Lyapunov exponents correspond to the peaks of the blue regions observed in the largest Lyapunov exponent plots. Interestingly, we find that as we continue to increment  $J$  beyond these green vertical strips, the percentage of positive Lyapunov exponents sharply declines.

The normalized Lyapunov dimension is shown in the bottom row of Figure 3. Here, we observe green and yellow vertical striations representing regions of reduced fractal dimensionality relative to the high fractal dimensionality red regions around them. These unstable dimension striations

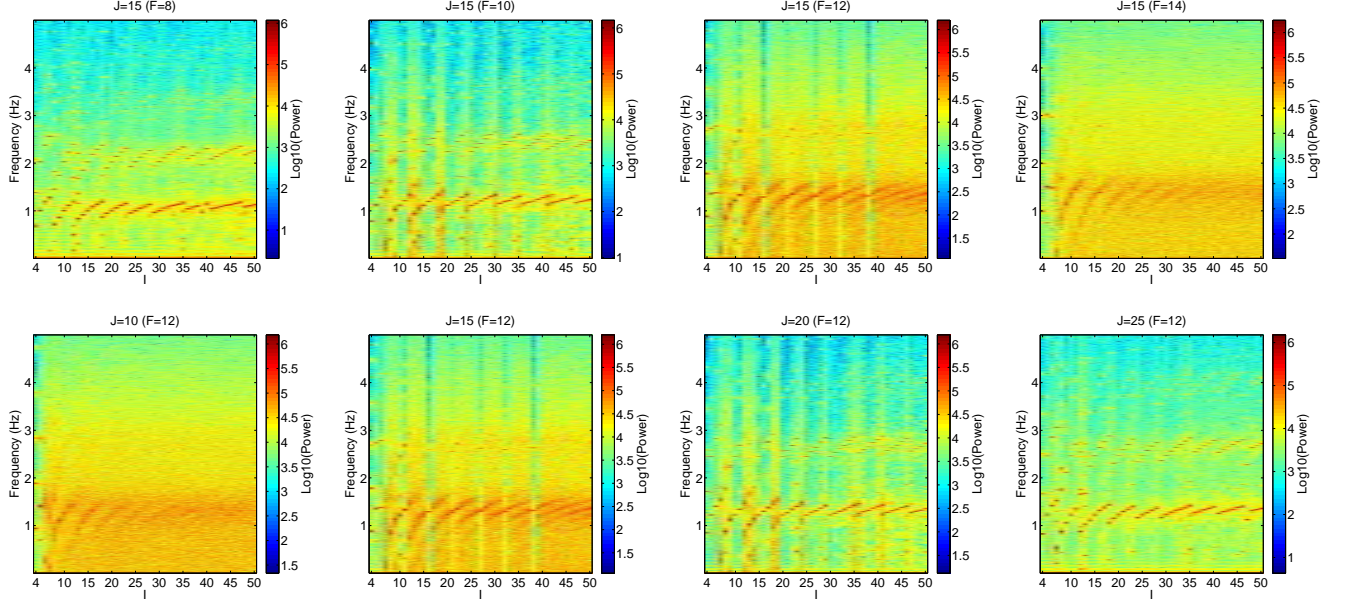


**Figure 4.** For these plots, the x-axis represents choices of  $I$ , the y-axis represents different frequencies, and the color represents the power spectrum of the trajectory of a slow oscillator at the corresponding parameter choice. (Top Row)  $J = 15$  while  $F \in [8, 10, 12, 14]$ . (Bottom Row)  $F = 12$  while  $J \in [10, 15, 20, 25]$ .

are in locations corresponding to the observed regions of reduced largest Lyapunov exponent, and the vertical striations of increased percentage of positive Lyapunov exponents. A periodicity in  $I$  is again apparent here.

We are surprised by these regions of reduced chaotic activity and endeavor to explore them using a frequency spectrum analysis. To this end, we examine frequency spectrum bifurcation diagrams representing slices through  $I$ - $J$  space with a fixed  $F$  [17]. Some of these slices are presented in Figure 4. We fix  $J = 15$  and increase the forcing  $F$  moving from left-to-right along the top row of Figure 4. Along the bottom row of Figure 4, We fix  $F = 12$  while increasing the number of fast variables  $J$  moving from left-to-right.

Examining the top row of Figure 4 for  $8 \leq F \leq 12$ , we find increased power at many frequencies for most choices of  $I$ , but, interestingly, we also observe periodic windows in the frequency spectrum bifurcation diagram where power is organized into just two different frequencies. Furthermore, these periodic windows of reduced spectral dispersion correspond to choices of  $I$  that resulted in stable behavior in Figure 3. We observe that when  $F \geq 14$  there is power at many frequencies for  $I \geq 6$  and periodic windows do not exist. This observation corresponds to the rise of the blue region of reduced largest Lyapunov exponent as  $F$  is increased (Figure 3).

We look at the frequency spectrum bifurcation diagram in the bottom row of Figure 4 by fixing  $F = 12$  and varying  $J$ . Figure 3 suggests that we will observe reduced largest Lyapunov exponent for  $10 \leq I \leq 35$  for most choices of  $I$ , and this is reflected in Figure 4 when we observe power at many frequencies for  $J = 10$ . We take steps through this region of reduced chaotic activity as we increase  $J$ , and again find periodic windows in the frequency spectrum bifurcation diagram, where large amounts of power are only found at a finite number of different frequencies. Again these windows of reduced spectral activity occur at  $I$  values corresponding to peaks in the blue regions from Figure 3. Furthermore, we see evidence that increasing  $J$  may have similar effects as reducing  $F$ .

Through further analysis of the frequency bifurcation spectrum diagrams, we observe that in general frequencies between one and two have more power, suggesting that slow oscillators tend to exhibit these frequencies even for parameter choices resulting in chaotic dynamics. We find more interesting frequency behavior in the many windows of organized spectral activity, where the dominant and subdominant frequencies, namely the frequency with the most power and the frequency with the second most power, appear to oscillate as a function of  $I$ . For  $J = 20$  and  $J = 25$  in the bottom row of Figure 4, we see that



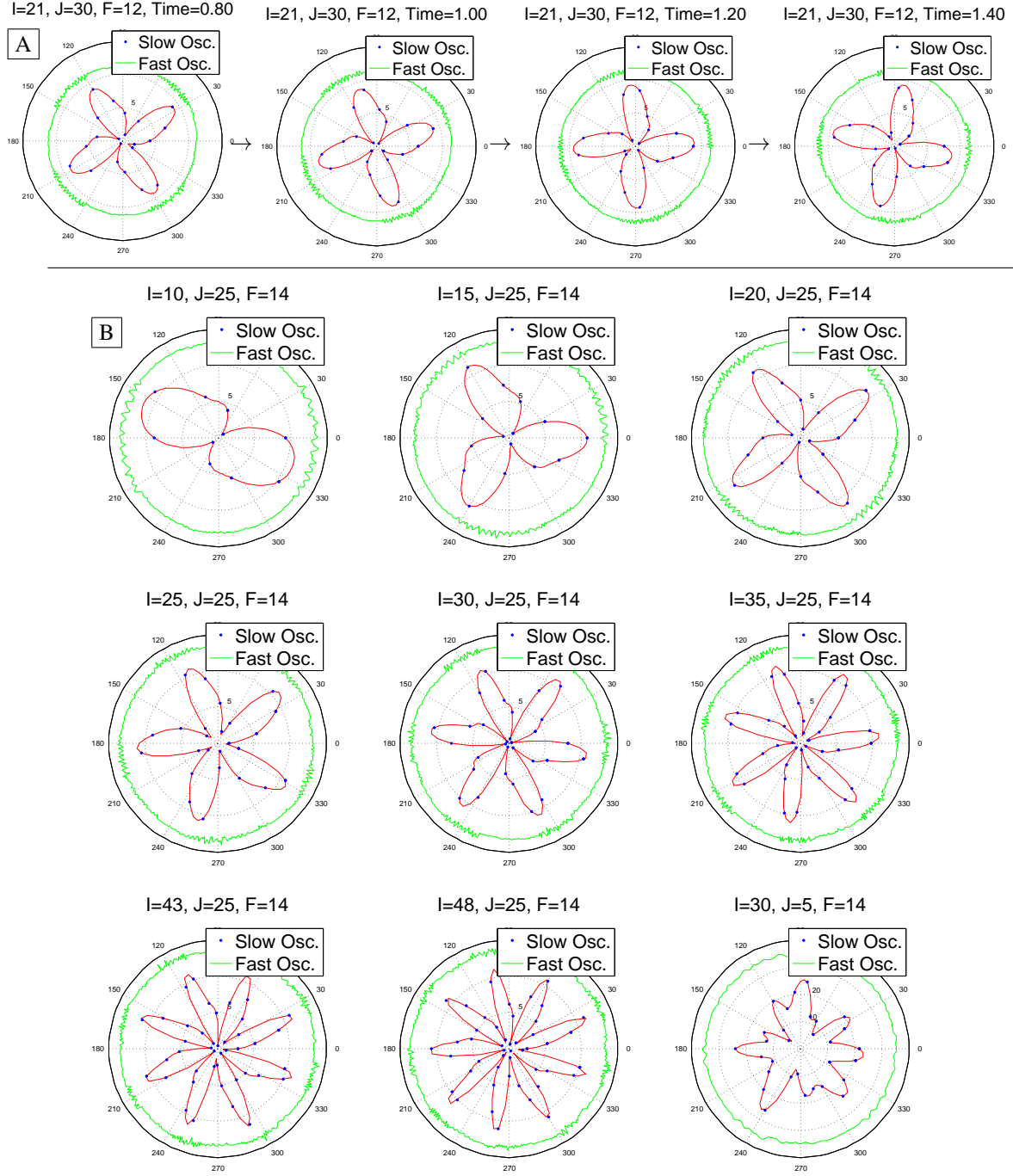


**Figure 5.** (A) For  $I = 21, J = 30$ , and  $F = 12$ , we plot the trajectories of the slow oscillators. This parameter choice yields a stable attractor as indicated by four snapshots of the standing waves, which travel clockwise around the ring of slow modes. (B) We show different parameter choices yielding different numbers of standing waves (from 2-9). The plot in the bottom right corner represents a snapshot of a trajectory on a chaotic attractor and shows much more irregularity than the standing waves. Animations of these time series can be found at <http://www.uvm.edu/storylab/share/papers/frank2014a/L96Stability.avi>

the dominant and subdominant frequencies fluctuate every fifth or sixth increment as we increase  $I$ . Also, the fluctuations become less severe as  $I$  approaches 50.

The frequency spectrum bifurcation diagrams show us that several parameter choices constrain the slow oscillators to two distinct frequencies. This suggests that we should see a strong regularity in the time series for these parameter choices. In Figure 5, we provide example snapshots of stable attractors, which resemble rose-plots in polar coordinates, and a chaotic attractor with a strong, positive largest Lyapunov exponent, which resembles an amoeba (bottom right). Each petal of the stable attractors is in fact a standing wave traveling around the slow oscillators over time as shown by Figure 5A. We see that the oscillations of the stable attractors show signs of being comprised of two frequencies, as individual slow os-

cillators seem to achieve both a relative local maximum and a global maximum. Furthermore, as we increase  $I$  we see additional petals added to the stable attractor. If  $I$  is chosen so that it falls between two windows of increased spectral organization, then we see the dynamics attempt to add an additional petal, but this petal will dissipate over time in a repeating process that prevents the trajectory from stabilizing. We propose a simple function describing the stable behavior in the Appendix.

We have provided evidence that stability emerges amongst regions of chaos in parameter space for the Lorenz '96 system, and that there appears to be a relationship between the usual bifurcation parameter,  $F$ , and the parameters controlling the dimension of the system,  $I$  &  $J$ . Figure 6 shows a few bifurcation diagrams where  $I$ , the number of slow oscillators, is used as a bifurcation

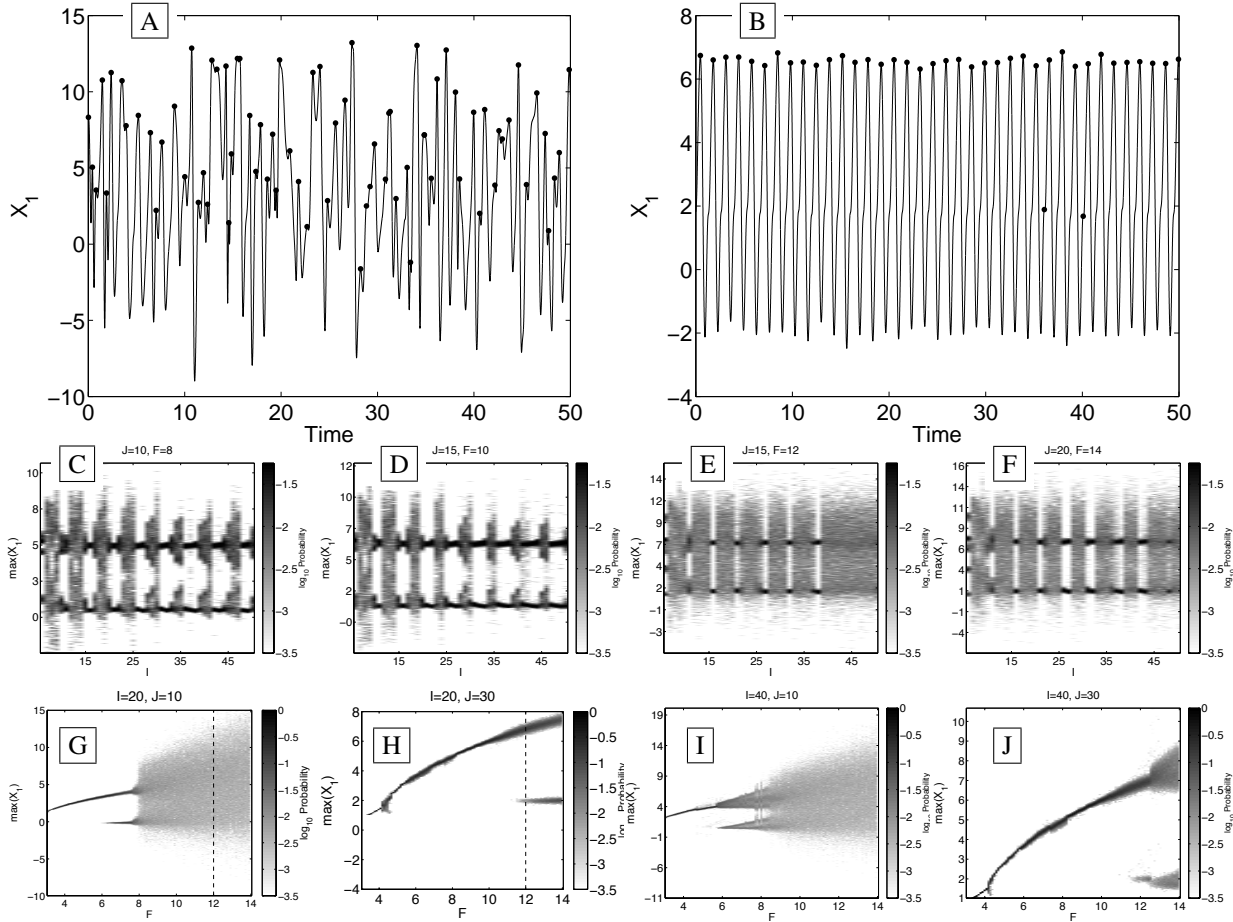


**Figure 6.** In the top row (A & B), we show two example trajectories representative of  $I = 20, J = 10, F = 12$  and  $I = 20, J = 30, F = 12$ , respectively. Black circles indicate local maxima of the trajectories. These time series are example trajectories taken from the bifurcation diagrams; panel A corresponds to the dashed line in panel G, and panel B corresponds to the dashed line in panel H. In the middle row (C-F), we provide bifurcation diagrams for several choices of  $J$  and  $F$  while  $I$  is varied as the bifurcation parameter. The y-axis indicates the values of the  $x_1$  local maxima. Note that ranges of the y-axes are different for each figure. The x-axis represents different choices of  $F$  in the bottom row (G-J) for a few choices of  $I$  and  $J$ . We observe both windows of stability and windows of chaos.

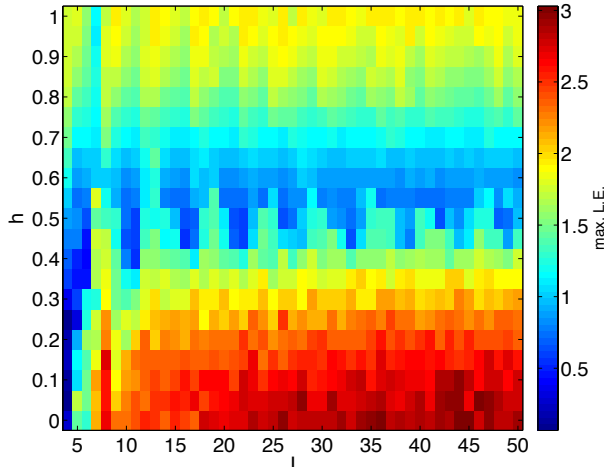


Figure 7. We examine the largest Lyapunov exponent as we vary  $I$  on the x-axis and  $h$ , the coupling parameter, on the y-axis.  $J$  is fixed to be 50. We find a pattern similar to the ones observed in Figure 3.

parameter. These bifurcation diagrams display clearly where regions of stability and chaos can be found as we tune  $I$ . Furthermore, we again observe evidence of the regularity in the trajectories of the slow oscillators for parameter choices leading to stability since the values of the local maxima of the slow oscillators in such regions are roughly constant across each bifurcation diagram.

Thinking of the dimensional parameters  $I$  and  $J$  as physical parameters, we provide bifurcation diagrams for different choices of  $I$ ,  $J$ , and  $F$ , along with two representative  $\bar{x}$  variable trajectories, in Figure 6. Figures 6A, 6B are example trajectories corresponding to the dashed lines in figures 6G, 6H, respectively. The dots in these time series indicate local maxima of the trajectories [3]. Figure 6A demonstrates that values of the local maxima can fluctuate wildly, while figure 6B shows a parameter choice for which local maxima tend towards only two different values. The middle row of Figure 6 (panels C-F) exhibits windows of both stable and chaotic dynamics as a function of the dimensional parameter  $I$ . We again observe windows of stability and chaos in panels G-J where  $F$ , a physical parameter, is tuned as the bifurcation parameter for several choices of  $I$  and  $J$ . For a fixed  $I$ , increasing  $J$  seems to condense the dynamics, constraining them to the envelope of values observed.

Figure 7 allows us to relate the effects of varying the dimensional parameter  $J$  to varying the physical coupling parameter  $h$ . We vary  $I$  from 4 to 50 and vary  $h$  from 0 to 1 while holding fixed  $J = 50$  (note that  $h = 1$  in all previous figures, consistent with the literature). We observe a pattern reminiscent of those observed in the top row of Figure 3, which suggests that the parameters  $h$  and  $J$  may have an analogous effect on the system.

## 4 Discussion

The Lorenz '96 model is a popular choice for atmospheric scientists attempting to improve prediction techniques. This is largely due to the reduction in degrees of freedom offered by the Lorenz '96 system in comparison to more sophisticated models used to make real-world weather predictions. Despite this simplification, the Lorenz '96 model is known for being a computationally manageable model that exhibits tunable levels of chaos, making it an appropriate tool for testing prediction techniques. However, our inspection of parameter space reveals regions of unexpected structural stability. In matters of complexity, it is common to assume that adding simple agents will only lead to more complexity, but in the case of the Lorenz '96 model we see that there exists a bounded range of  $J$  which organizes the dynamics and results in a dampening of system-wide chaos.

We attempt to explain the observed regions of stability by inspecting the equations for the Lorenz '96 system. Considering equation (2), the sum of the fast oscillators coupled with a given slow oscillator has a dampening effect on the velocity of the slow oscillator, while we also find that the slow oscillator provides positive feedback to the fast oscillators to which it is coupled in equation (3). Therefore, since each slow oscillator has many fast oscillators coupled with it, we expect any excitement of the slow oscillator to be quickly damped away by the fast oscillators. We find evidence of this in Figure 5, where peaks in the trajectories of the slow oscillators (points on the inner circle) correspond to increased activity in the fast oscillators coupled with it (the radially adjacent region in the outer circle). If one continues to increase  $J$  beyond the observed regions of stability, then the increasingly chaotic dynamics observed in Figure 3 may be a result of increased apparent forcing. The magnitude of the sum of the fast oscillators for a given slow oscillator may be large enough to act as a driving force for the dynamics of the slow oscillator (see equation (2)).

To test this theory, Figure 7 shows the largest Lyapunov exponents as we vary  $I$  and  $h$ , the coupling parameter, while holding  $J$  fixed at 50. Recalling equation (2), we see that reducing  $h$  dampens the sum of the fast oscillators coupled to each slow oscillator. We observe that Figure 7 exhibits a similar pattern to Figure 3, supporting the claim that reducing the sum of the fast oscillators leads to the stable behavior we observe.

The frequency spectrum bifurcation diagrams in Figure 4 reveal that the parameter choices for reduced chaotic activity in Figure 3 yield surprisingly regular stable attractors with slow oscillators whose trajectories are comprised



of only two frequencies. In fact, so long as the choices of  $I$ ,  $J$ , and  $F$  are such that the Lorenz '96 system is in one of the stable regions of parameter space, the trajectories of any slow oscillator exhibits approximately the same dynamics since the dominant and subdominant frequencies for stable attractors lie between 1-2, and 2.5-3, respectively, as seen in the frequency spectrum bifurcation diagrams in Figure 4. Indeed, the local maxima of the trajectories of the slow oscillators remain roughly constant across parameter choices leading to stability as shown in Figure 6. For a given choice of  $F$  and  $J$ , as  $I$  is increased from one stable region in parameter space to the next, we observe the addition of a petal, or a wave, to the attractor. When  $I$  lies in between regions of stability in parameter space, we observe attractors that periodically try to grow an additional petal that will eventually dissipate over time. These interesting attractor behaviors appear to occur periodically as a function of  $I$ .

### Acknowledgements

We would like to thank the Mathematics and Climate Research Network, the Vermont Complex Systems Center, and the Vermont Advance Computing Core for funding.

### Author Contributions

C.M.D., M.R.F. and L.M. designed the research. M.R.F. and C.M.D. prepared the figures and wrote the manuscript. M.R.F., L.M., and C.M.D analyzed the data and reviewed the manuscript.

### Competing Financial Interests

The authors declare no competing financial interests.

## References

- [1] R. A. Kerr. *Weather Forecasts Slowly Clearing Up*. Science 9 November 2012: Vol. 338 no. 6108 pp. 734-737 DOI: 10.1126/science.338.6108.734
- [2] J. A. Yorke. *Chaos: An Introduction to Dynamical Systems*. American Institute of Physics. ISSN: 0031-9228. <http://dx.doi.org/10.1063/1.882006>
- [3] Lorenz, Edward N., 1963: *Deterministic Nonperiodic Flow*. *J. Atmos. Sci.*, **20**, 130.141.
- [4] E. N. Lorenz. *The predictability of a flow which possesses many scales of motion*. **Tellus XXI**, 289 (1968).
- [5] Farmer, J. D., and J. J. Sidorowich. *Predicting Chaotic Time Series*. *Phys. Rev. Lett.* 59(8) (1987): 845-848.
- [6] C. M. Danforth, J. A. Yorke. 2006. *Making Forecasts for Chaotic Physical Processes*. *Physical Review Letters*, 96, 144102.
- [7] E.N. Lorenz, K.A. Emanuel, *Optimal sites for supplementary weather observations: simulation with a small model*, *J. Atmos. Sci.* 55 (1998) 399414.
- [8] E.N. Lorenz, *Predictability A problem partly solved*, in: ECMWF Seminar Proceedings on Predictability, Reading, United Kingdom, ECMWF, 1996, pp. 118.
- [9] D. S. Wilks, *Effects of Stochastic Parametrizations in the Lorenz 96 System*, *Quart. J. Roy. Meteor. Soc.* 131 (2005) 389407.
- [10] D. Orrell, *Role of the Metric in Forecast Error Growth: How Chaotic is the Weather?*, *Tellus* 54A (2002) 350362.
- [11] C. M. Danforth, E. Kalnay, *Using Singular Value Decomposition to Parameterize State-Dependent Model Errors*, *J. Atmos. Sci.* 65 (2008) 14671478.
- [12] R. Lieb-Lappen, C. M. Danforth. 2012. *Aggressive Shadowing of a Low-Dimensional Model of Atmospheric Dynamics*. *Physica D*. Volume 241, Issue 6, Pages 637648.
- [13] A. Karimi, M. R. Paul. *Extensive Chaos in the Lorenz-96 Model*. *Chaos* 20, 043105 (2010).
- [14] R. England. *Error estimates for Runge-Kutta type solutions to systems of ordinary differential equations*. *The Computer Journal* (1969) 12 (2): 166-170. doi: 10.1093/comjnl/12.2.166
- [15] J. Kaplan, J. Yorke, *Chaotic behavior of multidimensional difference equations*, in: H.-O. Peitgen, H.-O. Walther (Eds.), *Functional Differential Equations and Approximations of Fixed Points*, *Lecture Notes in Mathematics*, vol. 730, Springer, Berlin, 1979, pp. 228-237.
- [16] D. Orrell, 2003. *Model Error and Predictability over Different Timescales in the Lorenz '96 Systems*. *J. Atmos. Sci.*, 60, 2219.2228.
- [17] D. Orrell, L. A. Smith. *Visualizing Bifurcations in High Dimensional Systems: The Spectral Bifurcation Diagram*. *International Journal of Bifurcation and Chaos*, Vol. 13, No. 10 (2003) 3015-3027
- [18] H. Li, E. Kalnay, T. Myoshi, C. M. Danforth. 2009. *Accounting for Model Errors in Ensemble Data Assimilation*. *Monthly Weather Review*. 137, No. 10, 3407-3419. doi:10.1175/2009MWR2766.1

## 5 Appendix

### 5.1 Modelling the Stable Behavior

We attempt to further understand the stable behavior observed in the Lorenz 96 model by proposing a simple function. We model the normalized magnitude of a standing wave among the slow modes (as observed in Figure 5) with  $N(\approx I/5)$  waves at time  $t$  using

$$r(\theta, t) = \frac{\sin(N(\theta + 2\pi f \cdot t)) + 1}{2}.$$

where  $f$  is the frequency of a representative slow mode. The frequency of the slow mode can be obtained by looking at the dominant frequency from the spectra illustrated in Figure 4 (a function of  $I$  and  $F$ ). Scaling  $f$  by the frequency of sine ( $2\pi$ ) and by the number of waves ( $N$ ) will yield the desired angular velocity for the standing waves resulting from the model. Example waves resulting from the model at  $t = 0$  are presented in the figure below.

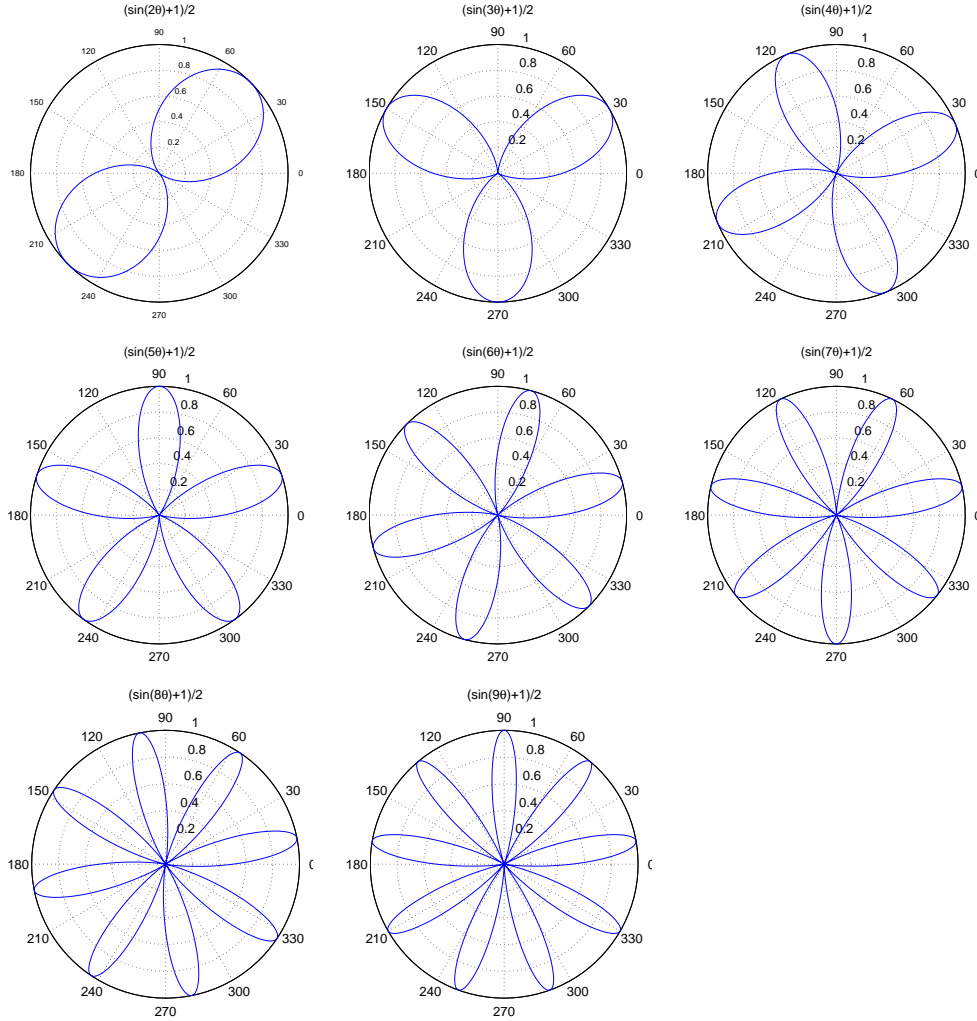


**Figure 8.** Example trajectories from the model for stable behavior. We examine the results from the model for  $t = 0$  with  $N \in \{2, 3, 4, 5, 6, 7, 8, 9\}$ . The resulting trajectories are comparable to the stable trajectories shown in Figure 5.